Int. J. Electrochem. Sci., 15 **(2020)** 5416 – 5429, doi: 10.20964/2020.06.72

International Journal of
ELECTROCHEMICAL
SCIENCE
www.electrochemsci.org

Mini Review

Two-dimensional Material as Anode for Lithium Ion Batteries: Recent Progress

Guang Huang[1*], *Bin Cai*[2*], *Changfa Zhan*[1] and Peng Sun[1]

[1] School of Conservation, Shanghai Institute of Visual Art, Songjiang 201620, Shanghai, P. R. China
[2] School of Chemistry and Chemical Engineering, Zhoukou Normal University, Zhoukou 466001, P. R. China
[*]E-mail: Guang Huang: guanghuang@aliyun.com Bin Cai: caib@actinide.org

Received: 21 January 2020 / *Accepted:* 23 March 2020 / *Published:* 10 May 2020

Compared with traditional bulk materials, two-dimensional nanomaterials exhibit peculiar physical and chemical properties. At present, two-dimensional nanomaterials have great application potential in the fields of medicine, aviation, energy and electronic information. To address both the energy and power demands of secondary LIBs for future energy storage applications, the development of innovative kinds of electrodes is required. In this review, we summarize the current development progress of two-dimensional materials used as anodes in lithium-ion batteries. Specifically, graphene, two-dimensional phosphorene, MoS_2 and MXene are highlighted.

Keywords: Two-dimensional material; MXene; Lithium ion batteries; MoS_2; Two-dimensional phosphorene; Graphene

1. INTRODUCTION

Broadly speaking, a two-dimensional material is a material that is much smaller in length in one dimension than the other two and can support itself. However, at present, there is no strict definition of the vertical dimension of materials for classification as two-dimensional materials. In a review on graphene published in 2007, a definition of graphene was provided. The electronic structure and physical properties of graphene are strongly related to the number of layers, so a material with a number of layers below 10 is defined as graphene, while those with more than 10 are classified as graphene [1–3]. Monolayer, bilayer and few-layer (three to ten layers) graphene are also classified as three different types of graphene crystals due to differences in electronic structure and properties. In addition to these traditional two-dimensional crystalline materials, researchers sometimes classify ultrathin nanowires that do not strictly meet the above definitions as two-dimensional materials [3,4]. Such ultrathin materials require a large transverse size and are ultrathin on the longitudinal scale (the thickness is less

than 5 nm), and atoms on the transverse scale can be arranged in a periodic manner, such as in ultrathin metals and ultrathin semiconductor, or irregular arrangement, such as in go and amorphous oxide.

The type and structure of battery electrode materials are directly related to the capacity of the battery and its lifespan [5,6]. At present, research on electrode materials at home and abroad is mainly concentrated on two aspects: one research direction seeks to further improve commercial electrode materials and their performance. The second seeks to explore and develop new electrode materials. Anode materials have always been considered the core part of lithium-ion batteries, so their performance is directly related to the overall performance of lithium-ion batteries. At present, commercial lithium-ion battery anode materials mainly have the following two problems. First, the theoretical capacity is low. Commercial $LiCoO_2$ anode materials have a capacity of approximately 140 mAh/g, while that of graphite cathode materials can reach 330 mAh/g, and the anode capacity is only approximately 50% of the cathode capacity [7,8]. Second, in terms of cost, anode materials account for more than 40% of the overall price, resulting in an uneven distribution of material costs [9–20]. Therefore, the research and development of high-capacity, low-cost cathode materials has very important practical significance.

With the gradual promotion of portable and flexible electronic products, it is of great practical significance to develop soft, high-performance and lightweight two-dimensional electrode materials. Flexible electronic devices will also be an emerging area in future electronic devices that can be embedded in a flexible matrix and withstand certain deformation without causing a large attenuation in capacity [21,22]. There are two main types of electrode materials in the current study: conductive collectors that act as self-supporting electrodes and self-supporting electrode materials with a two-dimensional layer structure [23–25].

Two-dimensional layered electrode materials mainly include graphene, metal sulfides (MoS_2, WS_2, and SnS_2), metal carbides (Ti_3C_2 and Ti_2C) and metal oxides (V_2O_5 and MoOs). Graphitic graphite has good mechanical properties and electrical conductivity [26,27]. It is an ideal two-dimensional flexible self-supporting electrode material. The direct use of graphene as an adhesive filter film to support a flexible conductive substrate is the most commonly used method. This method is simple, has mild preparation conditions, and is suitable for mass production; however, due to the presence of van der Waals forces, the graphene layer in the middle and the close packing of components result in a decrease in the effective utilization of surface area, and electrolyte transport will also be affected by certain restrictions. In this review, we summarize the current development progress of two-dimensional materials used as anodes in lithium-ion batteries [28,29]. Specifically, graphene, two-dimensional phosphorene, MoS_2 and MXene are highlighted.

2. GRAPHENE AS ANODE MATERIALS FOR LITHIUM ION BATTERIES

Graphene has good chemical stability, excellent electrical conductivity and mechanical flexibility. It can be used to modify electrode materials to produce highly conductive composite materials and improve electrochemical properties, especially multiplier properties. Graphene flakes can buffer the volume effect of metal or metal oxide anode materials during charge and discharge and improve

electronic conductivity, and graphene/metal (metal oxide) composites can be used as battery cathodes to improve multiplier performance and cycling performance.

Conductive modification of $LiFePO_4$ has been a research focus. Ding et al. [30] synthesized nanostructured $LiFePO_4$/graphene (1.5%) composites by coprecipitation at room temperature. The first discharge specific capacity was 160 mAh/g, while the 10.0 C discharge specific capacity was 110 mAh/g. Wang et al. [31] prepared $LiFePO_4$/graphene nanocomposites by a hydrothermal method and obtained a 0.1 C discharge specific capacity of 160.3 mAh/g and 10.0 C discharge specific capacity of 81.5 mAh/g. Raman spectroscopy analysis showed that the 8% graphene composite contained a high proportion of sp^2 hybrid carbon atoms, while the porous structure between $LiFePO_4$ particles and graphene nanosheets enabled the electrolyte to better penetrate the surface of the active material, which was conducive to improving electrochemical performance. Zhou et al. [32] modified $LiFePO_4$ with graphene, prepared a composite of $LiFePO_4$ nanoparticles and go by spray drying and heat treatment, and obtained spherical secondary particles with dimensions of 2 ~ 5 μm. The primary $LiFePO_4$ particles were uniformly and loosely coated by three-dimensional graphene sheets. Such nanostructures promote electron conduction in secondary particles, and the abundant gaps between $LiFePO_4$ particles and graphene flakes facilitate Li^+ migration, thus improving electrochemical performance. The discharge specific capacity at a 60 C ratio was still 70 mAh/g. After 1000 cycles, the capacity attenuation rate was less than 5%. Su et al. [33] prepared $LiFePO_4$/graphene and $LiFePO_4$/carbon black as cathode materials, and the electrochemical performance of composites containing 2% graphene was better than that of composites containing 20% carbon black. The main reason for these results is that the former material forms a "point-to-point" mode of conduction, which can better form a conductive network, while the latter material produces a "point-to-point" mode of conduction.

Compared to $LiFePO_4$, monoclinic $Li_3V_2(PO_4)_3$ has a higher voltage platform and higher specific capacity (approximately 197 mAh/g) but lower electronic conductivity (2.4 × 10.7 s/cm). Liu et al. [34] synthesized a $Li_3V_2(PO_4)_3$/GO complex by the sol-gel method. After reduction with ascorbic acid, a $Li_3V_2(PO_4)_3$/graphene nanocomposite was prepared. The discharge specific capacity was higher than 150 mAh/g, and the capacity retention rate after 100 cycles was 80%. Graphene nanosheets, acting as a two-dimensional conductive layer, were coated with $Li_3V_2(PO_4)_3$, preventing particle agglomeration, shortening the Li^+ diffusion path and enhancing electron conductivity.

$LiMnPO_4$ is a phosphate anode material with an olivine structure. The voltage platform is located at 4.1 V, matching that of many current liquid electrolytes. The energy density is approximately 20% higher than that of $LiFePO_4$, but the electronic conductivity is nearly 5 orders of magnitude lower than that of $LiFePO_4$. Wang et al. [35] prepared $LiMn_{0.75}Fe_{0.25}PO_4$ nanorods grown on graphene sheets by a solvothermal method, and the length of the nanorods was 50-100 nm. The stable specific capacities of the product at high multiplier rates of 20.0 C and 50.0 C were 132 mAh/g and 107 mAh/g, respectively, and the capacity decay rate at the 90th cycle was only 1.9%. This result is due to the graphene sheet coating of the active material, which reduces side reactions between the electrode and the electrolyte, forms a stable solid electrolyte phase interface film, and enhances electronic conductivity. Table 1 shows graphene-based anode materials and their electrochemical performances for use in lithium-ion batteries.

Table 1. Graphene-based anode materials and their electrochemical performances for lithium ion batteries.

Materials	Specific capacity and cyclic stability	Ref.
GNS + CNT	730 mAh/g at 0.05 A/g, 480 mAh/g after 20 cycles	[36]
Oxidized GNRs	1400 mAh/g at 0.05 A/g, 600 mAh/g after 10 cycles	[37]
MoS_2/graphene composite	1571 mAh/g at 0.1 A/g, 1187 mAh/g after 100 cycles	[38]
Fe_2O_3/rGO composite	1693 mAh/g at 0.1 A/g, 1027 mAh/g after 50 cycles	[39]
Crumpled graphene/MoO_3	1490 mAh/g at 2 A/g, 975 mAh/g after 10 cycles	[40]
Si/G	2158 mAh/g, 1168 mAh/g after 30 cycles	[41]
Si/G/carbon	2246 mAh/g at 0.1 A/g, 1000 mAh/g after 70 cycles	[42]
G/Si@CNFs	1792 mAh/g at 0.1 A/g, 897 mAh/g after 200 cycles	[43]
SnS_2/G-CNT	1743 mAh/g at 0.5 A/g, 798 mAh/g after 1000 cycles	[44]
Mn_3O_4/G	900 mAh/g was obtained after first 5 cycles at 40 mA/g	[45]
SnO_2/N-doped rGO	1865 mAh/g at 0.5 A/g, 1074 mAh/g after 500 cycles	[46]
SnO_2@P@GO	1278 mAh/g at 0.1 A/g, 550 mAh/g after 200 cycles	[47]
W-doped SnO_2/G	1240 mAh/g at 0.1 A/g, 808 mAh/g after 120 cycles	[48]
Sb_2O_3/rGO	2260 mAh/g at 0.1 A/g, 808 mAh/g after 120 cycles	[49]
Co_3O_4/G	1304 mAh/g at 0.2 A/g, 1113 mAh/g after 100 cycles	[50]

3. TWO-DIMENSIONAL PHOSPHORENE AS ANODE MATERIAL FOR LITHIUM ION BATTERIES

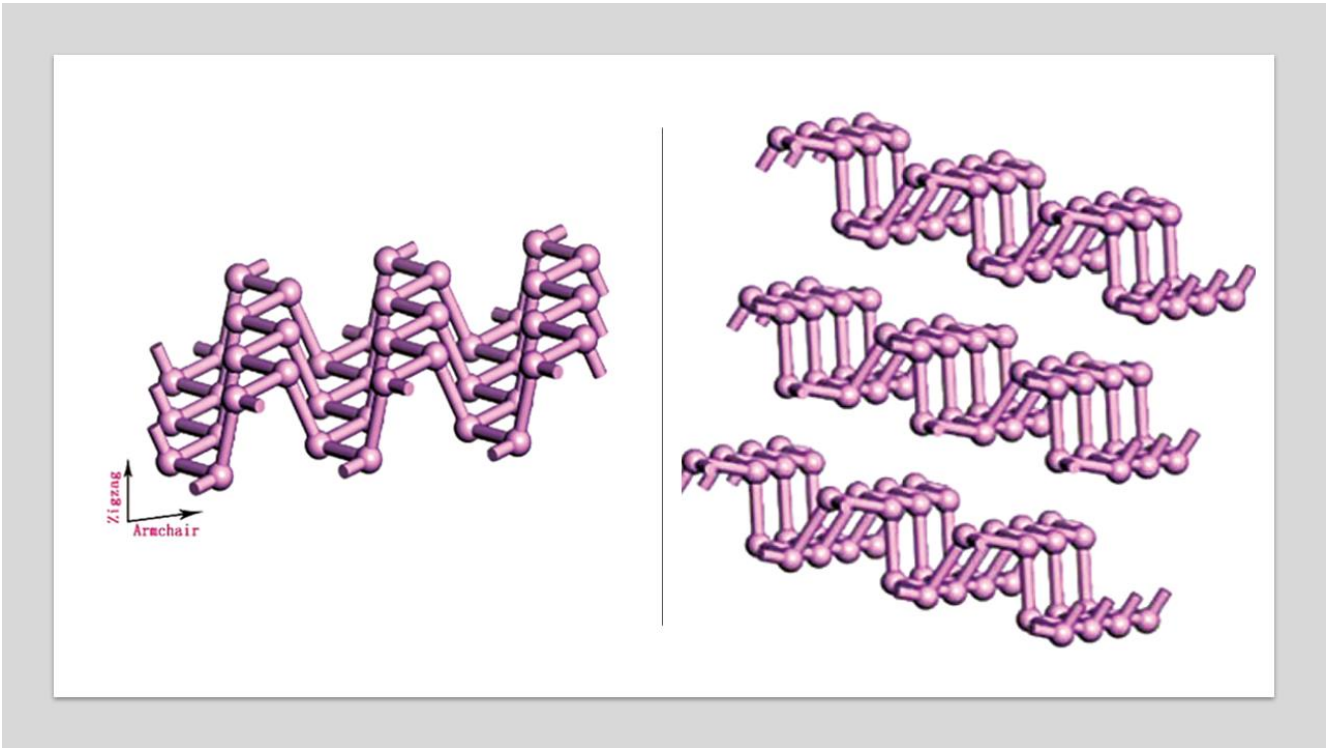

Figure 1. Schematic diagram of phosphorene.

Black phosphate can be mainly divided into four kinds of crystal structure: simple cubic, orthogonal, diamond and amorphous states [51]. Under atmospheric pressure, black phosphate crystals form an orthogonal crystal system with spindle morphology; the lengths in the three directions of a unit cell are a = 0. 33133 nm, b = 1. 0473 nm, c = 0. 4374 nm, and the layer spacing is approximately 0. 53 nm. Monolayer black phosphorus, also known as phosphorene, generally has a folded honeycomb structure [52,53]. Similar to the carbon atoms in graphene, each phosphorus atom is connected to three adjacent phosphorus atoms to form a stable ring structure. Each ring is made up of six phosphorus atoms, and because the bonding type is sp^2 hybridization, the combined bond structure of black phosphorus is stable at room temperature and pressure. The monolayers inside bulk black phosphorus interact with the weak van der Waals force [54,55], so black phosphorus can be obtained by mechanical stripping. The bulk black phosphorus structure and the phosphorene structure are shown in Figure 1.

Because the special folded structure of monolayer black phosphorus reduces its symmetry, black phosphorus crystals are anisotropic. Takao et al. measured the effective mass of black phosphorus carriers, and the effective mass of electrons and holes was $0.16m_0$ and $0.17m_0$, respectively, in the armchair direction and $0.81m_0$ and $0.71m_0$ in the zigzag direction. The Shirotani [56] resistivity of black phosphate crystals was measured, and the resistivity of single-layer black phosphorus in the two directions was 0.1 and 1 Ω·cm. In the vertical direction, the single-layer plane resistivity was Ω 102 ~ 103 cm. Zhe et al. [57] measured the thermal conductivity in the zigzag and armchair planes of low-layer black phosphorus by micro-Raman spectroscopy. The results showed that when the thickness of the black phosphorus film was greater than 15 nm, the thermal conductivity in the two directions of the monolayer black phosphorus plane was 40 and 20 W·m/k, respectively. As the thickness of the film decreased, the thermal conductivity in the two directions was reduced to 20 and 10 W·m/k, respectively. When the thickness of the film decreased to 9.5 nm, the anisotropic ratio decreased to 1.5 nm. Lee et al. [58] measured the thermal conductivity of black phosphorus under steady-state longitudinal heat flow by using a suspended pad microdevice. The study found that when the temperature exceeded 100 K, the anisotropy of thermal conductivity increased by two times, and the thinner the nanoribbon was, the lower the thermal conductivity. Because the anisotropy of black phosphorus is significant, it is very important to determine the crystal orientation of black phosphorus. Qiao et al. [59] calculated the bandgap, carrier mobility and anisotropy of black phosphorus by using density functional theory (DFT). The theoretical calculation results showed that the hole mobility of black phosphorus is greater than the electron mobility, and the middle valence band top and guide band bottom of the energy band structure are located at the same K point, indicating that black phosphorus is a p-type direct bandgap semiconductor. As the number of layers increased, the bandgap width gradually decreased from 1.51 eV for a monolayer to 0.59 eV for the block material. The cavity mobility in the armchair direction increased from 600 $cm^2 \cdot v/s$ in one layer to 4000 $cm^2 \cdot v/s$ in five layers. These properties indicate that the properties of black phosphorus can be regulated by changing the number of layers.

In theory, when the spacing of each layer of graphene in black phosphorus is larger, black phosphorus can store more charged ions; coupled with its special folded structure, which favors the storage of charged ions, the theoretical capacity of black phosphorus can reach 2596 mAh/g [60]. This value is almost 7 times the capacitance of graphite electrodes currently available on the market, so black phosphorus has huge potential for the future development of electrode materials.

Kulish et al. [61] studied the main trends in the changes in the electronic structure and mechanical properties of black phosphorus with the concentration of sodium ions by using first-principles calculations. The results showed that the adsorption energy of a single sodium atom to phosphorus is negative, indicating that the sodium-phosphorus interaction is good. In addition, the adsorption energy of phosphorus to sodium is much higher than the binding energy of sodium in the Na2 dimer and the binding energy of sodium in the block material, indicating that sodium atoms do not aggregate at low sodium concentrations. The specific capacitances of NaP and Na_2P were predicted by DFT to be 865 and 433 mAh/g, respectively. Although the diffusion of sodium ions in monolayer black phosphorus is anisotropic, the diffusion rates in both directions are acceptable. Considering its advantages of high stability, a high theoretical specific capacitance, a large active surface area and fast Na diffusion, black phosphorus is considered a very promising anode material for sodium-ion batteries. Although black phosphorus has a high theoretical capacitance, the capacitance declines substantially after the first cycle, which may be caused by poor electrical conductivity; this characteristic is a great challenge for the use of black phosphorus as an electrode material. Therefore, Jiang, etc. [62] used the direct chemical vapor deposition method in the growth of conductive carbon black phosphorus paper to create a high-performance black phosphorus-graphite anode for lithium-ion batteries; the battery anode had a high specific capacitance of 2168. 8 mAh/g and good cycle stability, and the specific capacitance after 200 cycles could still reach 1677. 3 mAh/g, so black phosphorus-graphite is expected to become the next generation of high-specific-capacitance lithium-ion battery cathode materials. Table 2 shows phosphorene-based anode materials and their electrochemical performances.

Table 2. Two dimensional phosphorene-based anode materials and their electrochemical performances for lithium ion batteries.

Materials	Specific capacity and cyclic stability	Ref.
Phosphorene–graphene	1306.7 mAh/g at 0.2 A/g, 1200 mAh/g after 800 cycles	[63]
C_3N/phosphorene	468.34 mAh/g at 0.02 A/g	[64]
Phosphorene ribbons	541 mAh/g (prediction)	[65]
Hexagonal boron nitride/blue phosphorene	801 mAh/g (prediction)	[66]
Blue phosphorene/MS_2	528.257 mAh/g (prediction)	[67]
Phosphorene	433 mAh/g (prediction)	[68]
Blue phosphorene/graphene	485 mAh/g (prediction)	[69]

4. MOS_2 AS ANODE MATERIAL FOR LITHIUM ION BATTERIES

The successful exploration and application of graphene have recently sparked widespread interest in graphene-like two-dimensional layered materials. Transition metallothionides (TMDs), especially TMDs at the depth of a single atomic layer, have emerged as a new class of nanomaterials for fundamental research and promising applications in the future. In TMDs, van der Waals forces are used

to stack MoS_2 layers together to form a sandwich structure in which a single MoS_2 layer is constructed of S-Mo-S atomic layers. Due to its inherent and thickness-related bandgap, MoS_2 is abundant in its natural form (molybdenite), which is one of the most promising semiconductor materials in recent years. In addition, MoS_2 crystals can be stripped into a single or several layers at the nanoscale in a number of ways, exhibiting unusual physical and electronic properties. For example, when the thickness of MoS_2 is reduced to a single layer, a transition occurs from an indirect bandgap to a direct bandgap. Specifically, when its thickness is reduced from that of the block material to a monolayer, due to the quantum limiting effect, the bandgap width will increase from 1.29 eV to approximately 1.80 eV, and the band structure will change from an indirect bandgap to a direct bandgap. Driven by these unique properties and advanced preparation methods, single-layer and low-layer MoS_2 nanosheets have been widely studied for electronic/optoelectronic sensors and energy storage and conversion devices.

As some of the most common TMD nanomaterials explored, MoS_2 nanomaterials have been used as structural units or substrates for the preparation of composites with other materials, such as organic materials, biomaterials, precious metals, metal oxides, metal sulfides, graphene and other carbon nanomaterials. In addition, the synergistic effect of two or more components can lead to some enhancement in performance or improved performance, which is very significant for improving electrochemical performance.

The high surface area to volume ratio of 2D MoS_2 nanosheets means that they are a subject of much research in lithium-ion battery design; for example, their ability to achieve tight electrode/electrolyte interactions and short diffusion paths for Li^+ ions has been investigated. For example, Chen et al. [70] introduced Fe_3O_4 nanoparticles into a MoS_2 wafer system to obtain satisfactory electrochemical performance. A flexible MoS_2/Fe_3O_4 composite electrode was synthesized by a hydrothermal method, and the morphology of the MoS_2 nanosheet was similar to that of graphene. In that work, a MoS_2 nanosheet was used as a flexible substrate, and Fe_3O_4 nanoparticles created a good compound anode barrier in the composite electrode. When used, the composites can adapt to volume changes during cycling, thus promoting electrolyte penetration and faster lithium ion transport. Moreover, in the subsequent electrochemical testing process, the battery constructed from this complex demonstrated outstanding endurance and power performance and achieved reversible capacities of 1033 mAh/g (2000 mA/g) and 224 mAh/g (10,000 mA/g). In addition, the combined micro/nano configurations of MoS_2 and metal oxides such as SnO_2 [71] and VO_2 [72] have been extensively explored. In general, metal oxides act as barriers and energy storage units in composite materials, not only hindering the aggregation of MoS_2 nanowires but also enabling the anode material to accommodate volume expansion during charging/discharging while providing a large capacity. In addition, modular electrodes based on a MoS_2- MOS hybrid system usually have excellent cycling durability. The above work fully proves that two-dimensional MoS_2 has great potential in the preparation of higher-energy-storage devices and as a flexible substrate. Table 3 shows MoS_2-based anode materials and their electrochemical performances for use in lithium-ion batteries.

Table 3. MoS_2-based anode materials and their electrochemical performances for lithium ion batteries.

Materials	Specific capacity and cyclic stability	Ref.
MoO_2@MoS_2	1000 mAh/g	[73]
MoS_2/Nanotube	1200 mAh/g, 950 mAh/g after 500 cycles at 2 A/g	[74]
Vertically aligned metallic MoS_2	1100 mAh/g at 5 A/g, 589 mAh/g after 350 cycles	[75]
Hierarchical MoS_2 tubular structures	1320 mAh/g at 0.1 A/g	[76]
Hierarchical MoS_2 hollow nanospheres	1150 mAh/g at 0.5 A/g	[77]
Synthesis of MoS_2@C Nanotubes	850 mAh/g at 5 A/g, 485 mAh/g after 500 cycles	[78]
MoS_2-TiO_2	648 mAh/g after 400 cycles	[79]
MoS_2 Nanosheets	1409 mAh/g at 0.1 A/g, 1230 mAh/g after 250 cycles	[80]
SnO_2-SnS/C nanosheets	1006 mAh/g at 0.2 A/g, 637 mAh/g after 500 cycles	[81]
Co_3S_4@C@MoS_2	672.6 mAh/g after 500 cycles	[82]
MoS_2/C	982 mAh/g after 100 cycles	[83]
MoS_2/C microspheres	1125.9 mAh/g, 916.6 mAh/g after 400 cycles	[84]
Co_9S_8@MoS_2	1298 mAh/g at 1 A/g, 1048 mAh/g after 300 cycles	[85]

5. MXene AS ANODE MATERIAL FOR LITHIUM ION BATTERIES

2D materials generally have the advantages of atomic-layer thickness, a large electrochemically active surface and excellent mechanical properties. In recent decades, 2D materials have attracted extensive attention from researchers in a variety of applications. In 2011, scientists discovered a new and rapidly expanding family of 2D transition metal carbides or carbonitrides. Such materials are named MXenes because of their graphene-like structural characteristics [86]. As shown in Figure 2, MXene materials are synthesized mainly by selectively etching out the "A" layer from the ternary-layered carbide and nitride MAX phase. The precursor MAX and etching product MXene are labeled $M_{n+1}AX_n$ and $M_{n+1}X_n$ T_x, where M, A, X and T represent early transition metals; IIIA or IVA group elements; C or N; and surface terminal functional groups (−O−, −OH, and −F), respectively. The value of N is generally from 1 to 3, and the number of terminal groups X is not determined [87]. At present, the MAX phase has more than 70 members and is increasing, thus ensuring the rich diversity of MXene materials. As one of the members of the MXene series, $Ti_3C_2T_x$ is one of the most fully studied and widely used. Based on mature etching and stripping techniques, $Ti_3C_2T_x$ has been able to produce stable structures with atomic-layer thickness and micron scale. The unique structural advantages of $Ti_3C_2T_x$ enable this material to replace other traditional layered materials, causing a new wave of research in 2D materials.

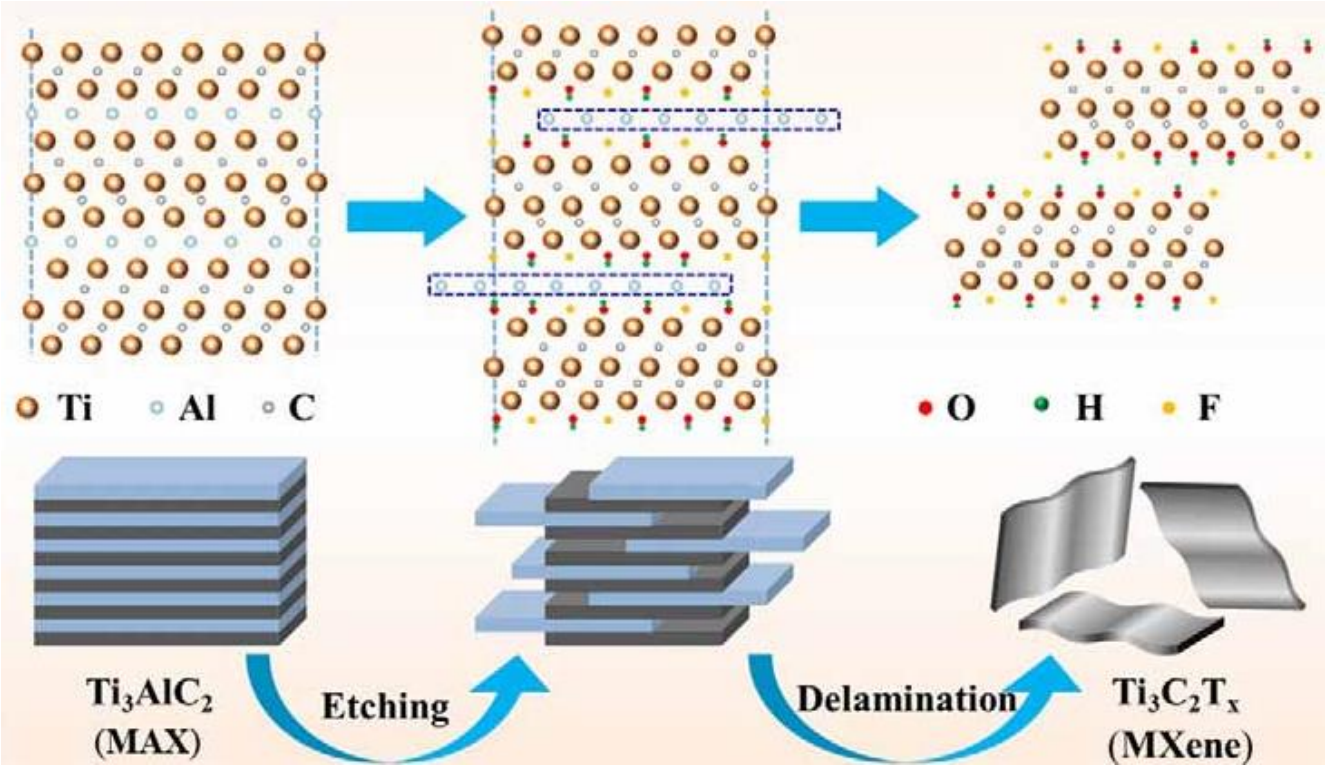

Figure 2. Synthetic process of the $Ti_3C_2T_x$ MXene.

Owing to its abundant surface functional groups, good thermodynamic stability, high conductivity, easy preparation and excellent chemical stability, MXene has been proven to be a promising material in a variety of applications. MXene has made some encouraging achievements in hydrogen storage [66], membrane separation [88], lithium-ion batteries [89], photocatalysis [90], supercapacitors [91], and Li-S batteries [92]. Recently, Zhang et al. [93], by directly mixing silicon powder with $Ti_3C_2T_x$ MXene ink, constructed a high-load MXene/Si composite electrode for lithium-ion batteries without an additional conductive agent and binder and achieved an area specific capacity of up to 23.3 mAh/cm^2, far exceeding those reported for negative electrodes of other lithium-ion batteries. Moreover, the MXene/Si composite electrode prepared by this method is simple, is fully compatible with the commercial coating process, can be produced on a large scale, and therefore has great potential application value.

Chen et al. [94] reported an effective strategy to construct $Ti_3C_2T_x$-based hydrogels based on a go-assisted self-convergence process. Under mild conditions, reductive $Ti_3C_2T_x$ reduced GO to reduced graphene oxide (RGO), which led to the sequential anisotropic assembly of a 3D RGO skeleton. Furthermore, due to the tight interfacial interaction between $Ti_3C_2T_x$ and RGO, $Ti_3C_2T_x$ self-converged into the framework, resulting in $Ti_3C_2T_x$-based hydrogels with interconnected porous networks. Due to the interconnected porous structure, the $Ti_3C_2T_x$ hydrogel shows excellent performance as a photocatalytic material.

Li et al. [95] successfully synthesized a $RuO_2{\cdot}xH_2O$@mxene nanocomposite by growing hydrated $RuO_2{\cdot}xH_2O$ nanoparticles in situ on the surface of $Ti_3C_2T_x$ MXene nanosheets by a water-phase synthesis method. The material can form a dynamic 3D network with one-dimensional silver

nanowires, thus facilitating the formation of electrode colloidal inks with high conductivity. Due to the unique structural design of the $RuO_2 \cdot xH_2O$@mxene nanocomposite, the excellent conductivity of the silver nanowire network, the synergy of the porous structure and high specific surface area, flexible microsupercapacitors constructed by screen printing technology showed excellent electrochemical performance. Among these supercapacitors, the volume specific capacity reached 864.2 F/cm^3, the highest value for printed microsupercapacitors reported so far. Table 4 shows MXene-based anode materials and their electrochemical performances for use in lithium-ion batteries.

Table 4. MXene-based anode materials and their electrochemical performances for lithium ion batteries.

Materials	Specific capacity and cyclic stability	Ref.
Titanium carbide MXene	100 mAh/g, 80 mAh/g after 500 cycles	[96]
Sn^{4+} ion decorated Ti_3C_2	1375 mAh/g	[97]
Silicon/MXene	2118 mAh/g at 0.02 A/g, 1672 mAh/g after 100 cycles	[98]
V_2C MXene	230.3 mAh/g at 0.02 A/g	[99]
$Li_4Ti_5O_{12}$-$Ti_3C_2T_x$	116 mAh/g at 5 A/g	[100]
titanium carbide/carbon nanotube	489 mAh/g at 0.1 A/g	[101]
Fe_3O_4@Ti_3C_2	747 mAh/g at 0.1 A/g, 278 mAh/g after 800 cycles	[102]
MXene supported Li_3VO_4	747 mAh/g	[103]

6. CONCLUSION

Two-dimensional materials have excellent physical and chemical properties, and they have shown great potential in energy conversion and storage, sensors and catalysis. Two-dimensional materials have many excellent properties and can be widely used in the future. In this review, we have summarized recent developments in two-dimensional materials for lithium-ion battery applications. Graphene, two-dimensional phosphorene, MoS_2 and MXene were the main focus.

ACKNOWLEDGEMENTS
This study was supported by Pei Ying Plan of SIVA (Z.30001.16.05.16.14), Shanghai Educational Science Planning Project (C19091) and the Key Scientific and Technological Research Projects in Henan Province (192102210028).

References

1. L. Wang, H. Liang, M. Xu, L. Wang, Y. Xie, Y. Song, *Sens. Actuators B Chem.*, 298 (2019) 126859.
2. P. Xiong, R. Ma, G. Wang, T. Sasaki, *Energy Storage Mater.*, 19 (2019) 281–298.

3. F. Shahzad, A. Iqbal, S.A. Zaidi, S.-W. Hwang, C.M. Koo, *J. Ind. Eng. Chem.*, 79 (2019) 338–344.
4. K.O. Oyedotun, D.Y. Momodu, M. Naguib, A.A. Mirghni, T.M. Masikhwa, A.A. Khaleed, M. Kebede, N. Manyala, *Electrochimica Acta*, 301 (2019) 487–499.
5. P. Pazhamalai, K. Krishnamoorthy, S. Sahoo, S.-J. Kim, *Electrochimica Acta*, 295 (2019) 591–598.
6. S. Wang, P. He, L. Jia, M. He, T. Zhang, F. Dong, M. Liu, H. Liu, Y. Zhang, C. Li, J. Gao, L. Bian, *Appl. Catal. B Environ.*, 243 (2019) 463–469.
7. Y. Tian, Y. Wang, L. Yan, J. Zhao, Z. Su, *Appl. Surf. Sci.*, 467–468 (2019) 98–103.
8. B. Xu, S. Qi, M. Jin, X. Cai, L. Lai, Z. Sun, X. Han, Z. Lin, H. Shao, P. Peng, Z. Xiang, J.E. ten Elshof, R. Tan, C. Liu, Z. Zhang, X. Duan, J. Ma, *Chin. Chem. Lett.*, 30 (2019) 2053–2064.
9. L. Fu, Z. Liu, J. Ge, M. Guo, H. Zhang, F. Chen, W. Su, A. Yu, *J. Electroanal. Chem.*, 841 (2019) 142–147.
10. L. Fu, A. Wang, G. Lai, C.-T. Lin, J. Yu, A. Yu, Z. Liu, K. Xie, W. Su, *Microchim. Acta*, 185 (2018) 87.
11. A. Baghizadeh, H. Karimi-Maleh, Z. Khoshnama, A. Hassankhani, M. Abbasghorbani, *Food Anal. Methods*, 8 (2015) 549–557.
12. T. Jamali, H. Karimi-Maleh, M.A. Khalilzadeh, *LWT - Food Sci. Technol.*, 57 (2014) 679–685.
13. H. Karimi-Maleh, F. Karimi, M. Alizadeh, A.L. Sanati, *Chem. Rec.*, n/a (2019).
14. H. Karimi-Maleh, A.F. Shojaei, K. Tabatabaeian, F. Karimi, S. Shakeri, R. Moradi, *Biosens. Bioelectron.*, 86 (2016) 879–884.
15. H. Karimi-Maleh, O.A. Arotiba, *J. Colloid Interface Sci.*, 560 (2020) 208–212.
16. S.A.R. Alavi-Tabari, M.A. Khalilzadeh, H. Karimi-Maleh, *J. Electroanal. Chem.*, 811 (2018) 84–88.
17. H. Rong, H. Hu, J. Zhang, J. Wang, M. Zhang, G. Qin, Y. Zhang, X. Zhang, *J. Mater. Sci. Technol.*, 35 (2019) 2485–2493.
18. L. Fu, M. Wu, Y. Zheng, P. Zhang, C. Ye, H. Zhang, K. Wang, W. Su, F. Chen, J. Yu, *Sens. Actuators B Chem.*, 298 (2019) 126836.
19. L. Fu, Y. Zheng, P. Zhang, H. Zhang, W. Zhuang, H. Zhang, A. Wang, W. Su, J. Yu, C.-T. Lin, *Biosens. Bioelectron.*, 120 (2018) 102–107.
20. Y. Lu, Y. Xu, H. Shi, P.Z.H. Zhang, L. Fu, *Int J Electrochem Sci*, 15 (2020) 758–764.
21. A. Jain, B.J. Paul, S. Kim, V.K. Jain, J. Kim, A.K. Rai, *J. Alloys Compd.*, 772 (2019) 72–79.
22. J. Wang, C. Yang, J. Wang, L. Han, M. Wei, *Electrochimica Acta*, 295 (2019) 246–252.
23. Y. Jin, J. He, Z. Ou, C. Feng, G. Zhang, *Chin. Chem. Lett.*, 30 (2019) 806–808.
24. Z. Wei, Z. Hai, M.K. Akbari, Z. Zhao, Y. Sun, L. Hyde, F. Verpoort, J. Hu, S. Zhuiykov, *Electrochimica Acta*, 297 (2019) 417–426.
25. J. Zhang, J. Wu, X. Zou, K. Hackenberg, W. Zhou, W. Chen, J. Yuan, K. Keyshar, G. Gupta, A. Mohite, P.M. Ajayan, J. Lou, *Mater. Today*, 25 (2019) 28–34.
26. J. Ju, J. Ma, Y. Wang, Y. Cui, P. Han, G. Cui, *Energy Storage Mater.*, 20 (2019) 269–290.
27. B. Saravanakumar, X. Wang, W. Zhang, L. Xing, W. Li, *Chem. Eng. J.*, 373 (2019) 547–555.
28. T. Sharifi, Y. Xie, X. Zhang, H.R. Barzegar, J. Lei, G. Coulter, S. Sun, C. Tiwary, A. Zettl, B. Yakobson, P.M. Ajayan, *Carbon*, 141 (2019) 266–273.
29. J. Zhu, B. Huang, C. Zhao, H. Xu, S. Wang, Y. Chen, L. Xie, L. Chen, *Electrochimica Acta*, 313 (2019) 194–204.
30. Y. Ding, Y. Jiang, F. Xu, J. Yin, H. Ren, Q. Zhuo, Z. Long, P. Zhang, *Electrochem. Commun.*, 12 (2010) 10–13.
31. L. Wang, H. Wang, Z. Liu, C. Xiao, S. Dong, P. Han, Z. Zhang, X. Zhang, C. Bi, G. Cui, *Solid State Ion.*, 181 (2010) 1685–1689.
32. X. Zhou, F. Wang, Y. Zhu, Z. Liu, *J. Mater. Chem.*, 21 (2011) 3353–3358.

33. F.-Y. Su, C. You, Y.-B. He, W. Lv, W. Cui, F. Jin, B. Li, Q.-H. Yang, F. Kang, *J. Mater. Chem.*, 20 (2010) 9644–9650.
34. H. Liu, P. Gao, J. Fang, G. Yang, *Chem. Commun.*, 47 (2011) 9110–9112.
35. H. Wang, Y. Yang, Y. Liang, L.-F. Cui, H. Sanchez Casalongue, Y. Li, G. Hong, Y. Cui, H. Dai, *Angew. Chem. Int. Ed.*, 50 (2011) 7364–7368.
36. E. Yoo, J. Kim, E. Hosono, H. Zhou, T. Kudo, I. Honma, *Nano Lett.*, 8 (2008) 2277–2282.
37. T. Bhardwaj, A. Antic, B. Pavan, V. Barone, B.D. Fahlman, *J. Am. Chem. Soc.*, 132 (2010) 12556–12558.
38. K. Chang, W. Chen, *ACS Nano*, 5 (2011) 4720–4728.
39. X. Zhu, Y. Zhu, S. Murali, M.D. Stoller, R.S. Ruoff, *ACS Nano*, 5 (2011) 3333–3338.
40. S.H. Choi, Y.C. Kang, *ChemSusChem*, 7 (2014) 523–528.
41. S.-L. Chou, J.-Z. Wang, M. Choucair, H.-K. Liu, J.A. Stride, S.-X. Dou, *Electrochem. Commun.*, 12 (2010) 303–306.
42. H. Li, C. Lu, B. Zhang, *Electrochimica Acta*, 120 (2014) 96–101.
43. X. Ma, G. Hou, Q. Ai, L. Zhang, P. Si, J. Feng, L. Ci, *Sci. Rep.*, 7 (2017) 1–8.
44. L. Zhang, Y. Huang, Y. Zhang, W. Fan, T. Liu, *ACS Appl. Mater. Interfaces*, 7 (2015) 27823–27830.
45. H. Wang, L.-F. Cui, Y. Yang, H. Sanchez Casalongue, J.T. Robinson, Y. Liang, Y. Cui, H. Dai, *J. Am. Chem. Soc.*, 132 (2010) 13978–13980.
46. X. Zhou, L. Wan, Y. Guo, *Adv. Mater.*, 25 (2013) 2152–2157.
47. L. Zhang, K. Zhao, R. Yu, M. Yan, W. Xu, Y. Dong, W. Ren, X. Xu, C. Tang, L. Mai, *Small*, 13 (2017) 1603973.
48. S. Wang, L. Shi, G. Chen, C. Ba, Z. Wang, J. Zhu, Y. Zhao, M. Zhang, S. Yuan, *ACS Appl. Mater. Interfaces*, 9 (2017) 17163–17171.
49. X. Zhou, Z. Zhang, X. Lu, X. Lv, G. Ma, Q. Wang, Z. Lei, *ACS Appl. Mater. Interfaces*, 9 (2017) 34927–34936.
50. Y. Yang, J. Huang, J. Zeng, J. Xiong, J. Zhao, *ACS Appl. Mater. Interfaces*, 9 (2017) 32801–32811.
51. A. Brown, S. Rundqvist, *Acta Crystallogr.*, 19 (1965) 684–685.
52. L. Cartz, S. Srinivasa, R. Riedner, J. Jorgensen, T. Worlton, *J. Chem. Phys.*, 71 (1979) 1718–1721.
53. J. Slater, G. Koster, J. Wood, *Phys. Rev.*, 126 (1962) 1307.
54. M. Baba, Y. Nakamura, Y. Takeda, K. Shibata, A. Morita, Y. Koike, T. Fukase, *J. Phys. Condens. Matter*, 4 (1992) 1535–1544.
55. S. Narita, Y. Akahama, Y. Tsukiyama, K. Muro, S. Mori, S. Endo, M. Taniguchi, M. Seki, S. Suga, A. Mikuni, *Phys. B C*, 117 (1983) 422–424.
56. Y. Takao, H. Asahina, A. Morita, *J. Phys. Soc. Jpn.*, 50 (1981) 3362–3369.
57. Z. Luo, J. Maassen, Y. Deng, Y. Du, R.P. Garrelts, M.S. Lundstrom, P.D. Ye, X. Xu, *Nat. Commun.*, 6 (2015) 8572.
58. S. Lee, F. Yang, J. Suh, S. Yang, Y. Lee, G. Li, H. Sung Choe, A. Suslu, Y. Chen, C. Ko, J. Park, K. Liu, J. Li, K. Hippalgaonkar, J.J. Urban, S. Tongay, J. Wu, *Nat. Commun.*, 6 (2015) 8573.
59. J. Qiao, X. Kong, Z.-X. Hu, F. Yang, W. Ji, *Nat. Commun.*, 5 (2014) 4475.
60. H. Hanna, W. Haiyan, T. Yougen, L. Younian, *Prog. Chem.*, 26 (2014) 572–581.
61. V.V. Kulish, O.I. Malyi, C. Persson, P. Wu, *Phys. Chem. Chem. Phys.*, 17 (2015) 13921–13928.
62. Q. Jiang, J. Li, N. Yuan, Z. Wu, J. Tang, *Electrochimica Acta*, 263 (2018) 272–276.
63. Y. Zhang, H. Wang, Z. Luo, H.T. Tan, B. Li, S. Sun, Z. Li, Y. Zong, Z.J. Xu, Y. Yang, K.A. Khor, Q. Yan, *Adv. Energy Mater.*, 6 (2016) 1600453.
64. G.-C. Guo, R.-Z. Wang, B.-M. Ming, C. Wang, S.-W. Luo, M. Zhang, H. Yan, *J. Mater. Chem. A*, 7 (2019) 2106–2113.
65. D. Wang, G.-C. Guo, X.-L. Wei, L.-M. Liu, S.-J. Zhao, *J. Power Sources*, 302 (2016) 215–222.

66. J. Bao, L. Zhu, H. Wang, S. Han, Y. Jin, G. Zhao, Y. Zhu, X. Guo, J. Hou, H. Yin, J. Tian, *J. Phys. Chem. C*, 122 (2018) 23329–23335.
67. Q. Peng, Z. Wang, B. Sa, B. Wu, Z. Sun, *ACS Appl. Mater. Interfaces*, 8 (2016) 13449–13457.
68. C. Zhang, M. Yu, G. Anderson, R.R. Dharmasena, G. Sumanasekera, *Nanotechnology*, 28 (2017) 075401.
69. Y. Li, W. Wu, F. Ma, *J. Mater. Chem. A*, 7 (2019) 611–620.
70. M. Armand, P. Touzain, *Proc. Fr. Am. Conf. Intercalation Compd. Graph.*, 31 (1977) 319–329.
71. L. Niu, K. Li, H. Zhen, Y. Chui, W. Zhang, F. Yan, Z. Zheng, *Small*, 10 (2014) 4651–4657.
72. H. Ramakrishna Matte, A. Gomathi, A.K. Manna, D.J. Late, R. Datta, S.K. Pati, C. Rao, *Angew. Chem. Int. Ed.*, 49 (2010) 4059–4062.
73. Z. Xu, T. Wang, L. Kong, K. Yao, H. Fu, K. Li, L. Cao, J. Huang, Q. Zhang, *Part. Part. Syst. Charact.*, 34 (2017) 1600223.
74. Y. Liu, X. He, D. Hanlon, A. Harvey, U. Khan, Y. Li, J.N. Coleman, *ACS Nano*, 10 (2016) 5980–5990.
75. Y. Jiao, A. Mukhopadhyay, Y. Ma, L. Yang, A.M. Hafez, H. Zhu, *Adv. Energy Mater.*, 8 (2018) 1702779.
76. Y.M. Chen, X.Y. Yu, Z. Li, U. Paik, X.W.D. Lou, *Sci. Adv.*, 2 (2016) e1600021.
77. Y. Wang, L. Yu, X.W. (David) Lou, *Angew. Chem. Int. Ed.*, 55 (2016) 7423–7426.
78. X. Zhang, X. Li, J. Liang, Y. Zhu, Y. Qian, *Small*, 12 (2016) 2484–2491.
79. B. Chen, E. Liu, T. Cao, F. He, C. Shi, C. He, L. Ma, Q. Li, J. Li, N. Zhao, *Nano Energy*, 33 (2017) 247–256.
80. L. Ma, B. Zhao, X. Wang, J. Yang, X. Zhang, Y. Zhou, J. Chen, *ACS Appl. Mater. Interfaces*, 10 (2018) 22067–22073.
81. Q. Pan, F. Zheng, X. Ou, C. Yang, X. Xiong, M. Liu, *Chem. Eng. J.*, 316 (2017) 393–400.
82. J. Dai, J. Li, Q. Zhang, M. Liao, T. Duan, W. Yao, *Mater. Lett.*, 236 (2019) 483–486.
83. Z. Wang, G. Wei, K. Ozawa, Y. Cai, Z. Cheng, H. Kimura, *Electrochimica Acta*, 239 (2017) 74–83.
84. Q.Q. Xiong, Z.G. Ji, *J. Alloys Compd.*, 673 (2016) 215–219.
85. K. Yang, T. Mei, Z. Chen, M. Xiong, X. Wang, J. Wang, J. Li, L. Yu, J. Qian, X. Wang, *Nanoscale*, 12 (2020) 3435–3442.
86. M. Naguib, M. Kurtoglu, V. Presser, J. Lu, J. Niu, M. Heon, L. Hultman, Y. Gogotsi, M.W. Barsoum, *Adv. Mater.*, 23 (2011) 4248–4253.
87. M. Naguib, O. Mashtalir, J. Carle, V. Presser, J. Lu, L. Hultman, Y. Gogotsi, M.W. Barsoum, *ACS Nano*, 6 (2012) 1322–1331.
88. J. Wang, P. Chen, B. Shi, W. Guo, M. Jaroniec, S.-Z. Qiao, *Angew. Chem. Int. Ed.*, 57 (2018) 6814–6818.
89. C. Chen, X. Xie, B. Anasori, A. Sarycheva, T. Makaryan, M. Zhao, P. Urbankowski, L. Miao, J. Jiang, Y. Gogotsi, *Angew. Chem. Int. Ed.*, 57 (2018) 1846–1850.
90. Y. Chen, X. Xie, X. Xin, Z.-R. Tang, Y.-J. Xu, *ACS Nano*, 13 (2019) 295–304.
91. T. Zhao, J. Zhang, Z. Du, Y. Liu, G. Zhou, J. Wang, *Electrochimica Acta*, 254 (2017) 308–319.
92. Z. Xiao, Z. Yang, Z. Li, P. Li, R. Wang, *ACS Nano*, 13 (2019) 3404–3412.
93. C. (John) Zhang, S.-H. Park, A. Seral-Ascaso, S. Barwich, N. McEvoy, C.S. Boland, J.N. Coleman, Y. Gogotsi, V. Nicolosi, *Nat. Commun.*, 10 (2019) 849.
94. Y. Chen, X. Xie, X. Xin, Z.-R. Tang, Y.-J. Xu, *ACS Nano*, 13 (2019) 295–304.
95. H. Li, X. Li, J. Liang, Y. Chen, *Adv. Energy Mater.*, 9 (2019) 1803987.
96. A. Byeon, M.-Q. Zhao, C.E. Ren, J. Halim, S. Kota, P. Urbankowski, B. Anasori, M.W. Barsoum, Y. Gogotsi, *ACS Appl. Mater. Interfaces*, 9 (2017) 4296–4300.
97. J. Luo, X. Tao, J. Zhang, Y. Xia, H. Huang, L. Zhang, Y. Gan, C. Liang, W. Zhang, *ACS Nano*, 10 (2016) 2491–2499.
98. Y. Tian, Y. An, J. Feng, *ACS Appl. Mater. Interfaces*, 11 (2019) 10004–10011.

99. F. Liu, Y. Liu, X. Zhao, K. Liu, H. Yin, L.-Z. Fan, *Small*, n/a (2020) 1906076.
100. J. Wang, S. Dong, H. Li, Z. Chen, S. Jiang, L. Wu, X. Zhang, *J. Electroanal. Chem.*, 810 (2018) 27–33.
101. P. Yu, G. Cao, S. Yi, X. Zhang, C. Li, X. Sun, K. Wang, Y. Ma, *Nanoscale*, 10 (2018) 5906–5913.
102. Y. Wang, Y. Li, Z. Qiu, X. Wu, P. Zhou, T. Zhou, J. Zhao, Z. Miao, J. Zhou, S. Zhuo, *J. Mater. Chem. A*, 6 (2018) 11189–11197.
103. Y. Huang, H. Yang, Y. Zhang, Y. Zhang, Y. Wu, M. Tian, P. Chen, R. Trout, Y. Ma, T.-H. Wu, Y. Wu, N. Liu, *J. Mater. Chem. A*, 7 (2019) 11250–11256.